Available online at www.sciencedirect.com
SCIENCE DIRECT
Journal of Catalysis 229 (2005) 352–364
JOURNAL OF CATALYSIS
www.elsevier.com/locate/jcat

MoS_2 morphology and promoter segregation in commercial Type 2 Ni–Mo/Al_2O_3 and Co–Mo/Al_2O_3 hydroprocessing catalysts

S. Eijsbouts [a,*], L.C.A. van den Oetelaar [b], R.R. van Puijenbroek [b]

[a] *Albemarle Catalysts, Research Centre, P.O. Box 37650, 1030BE Amsterdam, The Netherlands*
[b] *Akzo Nobel, Research and Technology Chemicals, P.O. Box 9300, 6800SB Arnhem, The Netherlands*

Available online 23 December 2004

Abstract

A series of commercial liquid-phase-sulfided Type 2 Ni–Mo/Al_2O_3 and Co–Mo/Al_2O_3 catalysts used in different trickle-phase reactions has been characterized by (scanning) transmission electron microscopy combined with energy-dispersive X-ray analysis ((S)TEM-EDX) and X-ray diffraction (XRD) analysis. In contrast to what is reported for H_2S/H_2 sulfided Type 2 model catalysts, MoS_2 stacking is not prominent in liquid-phase sulfided Type 2 commercial catalysts. The presence or absence of MoS_2 stacking has been shown to be highly dependent on the sulfidation procedure applied. Although Type 2 commercial Ni–Mo catalysts have high MoS_2 dispersion, there is a significant Ni sulfide segregation. This is not the case for their Co-containing counterparts.

Keywords: Molybdenum sulfide; Nickel sulfide; Cobalt sulfide; Hydrotreating catalysts; Sulfidation; (Scanning) transmission electron microscopy–energy-dispersive X-ray analysis ((S)TEM-EDX); X-ray diffraction analysis (XRD); Morphology; Stacking; Segregation

1. Introduction

Gasoline and diesel specifications continue to tighter, moving toward ultraclean fuels (< 10 ppm S) as the standard by the end of this decade. The commercial Type 2 catalysts discussed in the present paper are high-performance catalysts, having been specifically developed to meet these future fuel targets in existing refinery processes and units.

It is an accepted concept that the active phase in hydroprocessing catalysts consists of MoS_2 structures decorated with the promoter (Ni or Co) sulfide, the so-called Ni–Mo–S or Co–Mo–S phase [1–7]. Two types of these phases are described, Types 1 and 2 [3–7], but there is still confusion about the definition of these phases [8]. Type 2 is characterized by lower active phase-support interaction and, consequently, by a more complete sulfidation [3–7]. Type 2 model catalysts studied in the literature are mostly prepared by coimpregnation with nitrilo triacetic acid (NTA) followed by H_2S/H_2 sulfidation [2–4,9–16]. Ni sulfidation is delayed because of the application of NTA, resulting in the simultaneous sulfidation of the promoter and Mo and, therefore, in less promoter segregation [12,13,16]. In addition, these catalysts often contain MoS_2 stacks [1,3,4,17,18]. The intrinsic activity of the Type 2 active sites is higher compared with Type 1 [2–7].

The commercial Type 2 catalysts are different from the NTA model catalysts. They have much higher metal loadings and are mostly liquid phase sulfided. As in NTA model catalysts, no strong interaction with the support can be formed because of preparation conditions. The commercial Type 2 catalysts are also fully sulfided; their sulfidation is complete at lower temperatures, and the sulfidation of Ni is delayed compared with conventional catalysts [19]. The intrinsic activity of the commercial Type 2 catalysts is higher than those of conventional Type 1 and mixed Type 1/2 catalysts [20,21].

The promoter and support effects as well as the structure and morphology of the active phase in sulfidic Type 1 and Type 2 catalysts have been the subject of numerous studies [1,18,22–25]. Among other things, it was found that Co_9S_8 [26–28] and Ni sulfide [29–32] segregate under reaction conditions. Different Ni sulfides can be formed, depending on

* Corresponding author.
E-mail address: sonja.eijsbouts@albemarle.com (S. Eijsbouts).

0021-9517/$ – see front matter
doi:10.1016/j.jcat.2004.11.011

the reaction conditions; Ni_3S_2 is the most stable [11,30,31, 33–37]. The segregated Co_9S_8 and Ni_3S_2 are proposed to have a distinct catalytic role, providing spillover hydrogen for the MoS_2 active phase, in the "Remote Control" concept [26,30,38]. Different MoS_2 morphologies, including straight and curved MoS_2 single slabs and stacks, are observed in supported and unsupported catalysts [18,22,24,39–48]. The MoS_2 structures can be parallel [39,46,47,49–53] or perpendicular [44,49,51,54] to the support. The observed morphology and orientation differences are related to active phase composition, type of support, presence of additives (such as phosphorus), preparation variables, and sulfidation and reaction conditions applied [1,18,22–25].

The present paper will demonstrate that Ni sulfide segregation occurs in both commercial Types 1 and 2 Ni–Mo catalysts under reaction conditions, even though the Ni sulfidation is delayed in Type 2 catalysts. In addition, it will be shown that MoS_2 stacks are not prominent in liquid-phase-sulfided commercial Type 2 catalysts.

2. Experimental

2.1. Samples

The categorization Types 1, 1/2, and 2 used in the present paper is based on the catalyst preparation procedure. Type 1 catalysts are typically P-free calcined catalysts. Most of the conventionally prepared calcined catalysts contain in fact a mixture of Types 1 and 2 phases [8] and are therefore referred to as Type 1/2 in the text. Type 1/2 catalysts are, for example, low-temperature calcined or dried catalysts with a low P content, which contain a mixture of Types 1 and 2 phases. Catalysts with a higher intrinsic activity are referred to as Type 2 catalysts when they are prepared in a way preventing any strong interaction with the support. Type 2 catalysts are low-temperature calcined or dried catalysts typically with a high P content and/or an organic additive. Types 1 and 1/2 catalysts are further characterized by incomplete sulfidation, and Type 2 catalysts are fully sulfided [19]. The intrinsic activity is higher for Type 2 compared with Type 1 catalysts. Types 1/2 and 2 hydroprocessing catalysts studied in this paper are representative examples of a much larger set of catalysts and are based on proprietary as well as competitive technologies. All samples contain P (0.3 to 4.5 at/nm^2). The samples are listed in Table 1 together with the annotations used in the text. The annotations contain references to the catalyst type (T1/2 and T2 refer to Types 1/2 and 2, respectively), sulfidation procedure (L and G refer to liquid-phase and gas-phase sulfidation, respectively), and reaction conditions (using annotations from Tables 1 and 2).

The following liquid-phase sulfidation procedure was applied for all catalysts except NiMo3-T2-G-H, NiMo3-T2-G, and CoMo3-T1/2-L-D. After the unit was pressure tested at room temperature (RT), the catalyst was soaked with presulfiding oil (dimethyl disulfide (DMDS)-spiked straight run gas oil (SRGO) containing in total 3.7 wt% S) for 3 h at RT in the presence of hydrogen. Liquid-phase presulfiding was then carried out under the following conditions: liquid hourly space velocity (LHSV) of 3.0 h^{-1}, H_2/oil ratio (H_2/oil) of 200 Nl/l, and 45 bar total pressure. The temperature was increased at 30 °C/h to 250 °C and kept at 250 °C for 8 h. The temperature was then further increased at 20 °C/h to 320 °C and kept at 320 °C for 5 h. After the presulfiding was finished, the feed was switched and the reaction pressure and temperature were adjusted to the required operating conditions.

NiMo3-T2-G-H was gas phase sulfided with an H_2S/H_2 mixture (2 °C/min to 300 °C, 4 h at 300 °C) prior to the above liquid-phase sulfidation procedure. SRGO feedstock (1.2 wt% S), which was not spiked with DMDS, was used in the liquid-phase start-up of the H_2S/H_2 sulfided catalysts. NiMo3-T2-G was gas-phase sulfided with an H_2S/H_2 mixture (360 °C/h to 400 °C, 2 h at 400 °C). CoMo3-T1/2-L-D was sulfided with the above liquid-phase sulfidation procedure, with the only difference that the total pressure was 30 bar instead of 45 bar.

The samples originated from various activity tests (Tables 1 and 2). All tests except for the FCC-PT canister were carried out in trickle-flow reactor units, with 100 ml of catalyst. The FCC-PT canister (1-liter cubic basket made of stainless-steel wire mesh) was placed in the commercial refinery unit. The reaction conditions in different applications are listed in Table 2. The severity of the conditions increases from the left to the right in Table 2.

2.2. Analytical methods

2.2.1. (S)TEM-EDX

The samples were extracted with toluene prior to being powdered, evacuated for at least 2 h at 150 °C, and subsequently vacuum impregnated with a standard mixture (Ultra Low Viscosity Kit, hard version; Polaron Instruments Inc.). The mixture was transferred into a polyethylene capsule (BEEM) and mixed with fresh embedding medium. The epoxy embedding medium was hardened for at least 48 h under N_2 (0.2 MPa, 338 K). Sections of about 60-nm thickness were prepared with a Leica Reichert Ultracut-S ultramicrotome, collected on a water surface, and transferred to a slightly etched (Ar plasma) Cu grid and dried. The thin sections on the TEM grid were covered with a thin layer of carbon to prevent charging during TEM analysis. Shortly after preparation, the sections were investigated with a JEOL JEM-2010F-HR TEM, with a 200-kV electron beam (field emission gun, FEG) and equipped with a STEM unit and a Thermo Noran EDX system.

MoS_2 morphology was studied by TEM imaging under slightly underfocused conditions. Semiquantitative evaluation of the MoS_2 features in the TEM micrographs was carried out using a method detailed elsewhere [29,55]. For each catalyst, all of the high-dispersion micrographs

Table 1
Catalyst properties

Catalyst annotation[a]	Description	Metal loadings	Sulfidation	Originating from [b]
NiMo1-T2-L-F	Type 2 Ni–Mo/Al_2O_3	3.2 at Ni and 5.8 at Mo per nm^2	Liquid phase	FCC-PT
NiMo2-T2-L-F	Type 2 Ni–Mo/Al_2O_3	1.8 at Ni and 5.6 at Mo per nm^2	Liquid phase	FCC-PT
NiMo3-T2-L-U	Type 2 Ni–Mo/Al_2O_3	2.5 at Ni and 8.1 at Mo per nm^2	Liquid phase	ULSD
NiMo3-T2-L-F/C	Type 2 Ni–Mo/Al_2O_3	2.5 at Ni and 8.1 at Mo per nm^2	Liquid phase	FCC-PT canister
NiMo3-T2-G-H	Type 2 Ni–Mo/Al_2O_3	2.5 at Ni and 8.1 at Mo per nm^2	Gas phase	HC-PT
NiMo3-T2-G	Type 2 Ni–Mo/Al_2O_3	2.5 at Ni and 8.1 at Mo per nm^2	Gas phase	–
NiMo4-T1/2-L-F	Type 1/2 Ni–Mo/Al_2O_3	1.5 at Ni and 3.1 at Mo per nm^2	Liquid phase	FCC-PT
CoMo1-T2-L-F	Type 2 Co–Mo/Al_2O_3	1.7 at Co and 4.8 at Mo per nm^2	Liquid phase	FCC-PT
CoMo2-T2-L-U	Type 2 Co–Mo/Al_2O_3	2.4 at Co and 6.7 at Mo per nm^2	Liquid phase	ULSD
CoMo3-T1/2-L-D	Type 1/2 Co–Mo/Al_2O_3	1.5 at Co and 3.1 at Mo per nm^2	Liquid phase	Diesel HDS

[a] Type 1/2 (T1/2), Type 2 (T2), liquid phase sulfidation (L), gas phase sulfidation (G), FCC-PT (F), ULSD (U), FCC-PT canister (F/C), HC-PT (H), diesel HDS (D).
[b] Fluid catalytic cracker pretreat (FCC-PT), ultra low sulfur diesel (ULSD), hydrocracker pretreat (HC-PT), hydrodesulfurization (HDS).

Table 2
Reaction conditions

	Diesel HDS[a]	ULSD	FCC-PT	HC-PT	FCC-PT canister
Annotation	D	U	F	H	F/C
Temperature (°C)	340	340	360	380	410
Pressure (bar)	30	45	70	100	57
H_2:oil (h^{-1})	120	400	400	1000	380
LHSV	4	2.5	1.2	2.0	0.7
Test duration	5 days	5 days	7 days	8 days	Ca. 1 year
Feed[b]	SRGO	LGO	VGO	CGO	HVGO

[a] HDS = hydrodesulfurization.
[b] LGO = light gas oil, VGO = vacuum gas oil, CGO = coker gas oil, HVGO = heavy vacuum gas oil.

available were included in the semiquantitative evaluation. Typically, at least five micrographs (each corresponding to ca. 5500 nm^2) were evaluated for each type of area present in the catalyst, that is, 10 to 15 micrographs were evaluated for inhomogeneous catalysts. This method, developed for an older generation of Types 1 and 1/2 catalysts and for an older TEM instrument, was used without further modification to evaluate the images of the present Type 2 catalysts. The calculation method includes assumptions related to the thickness of the specimen that is imaged and the tilt range in which MoS_2 structures are visible. These assumptions may depend on the exact TEM apparatus/settings and TEM specimen preparation applied. As the quality of the TEM micrographs has significantly improved over the years and as the Type 2 catalysts have a number of specific morphological features, it may be necessary to adjust some of the assumptions used in the calculations. This is under investigation at present. Even though the absolute values for the number of Mo edge and corner (e + c) sites may be adjusted, the trend within specific catalyst series is not expected to change. The same applies if a part of MoS_2 has a morphology different from a perfect hexagon (e.g., a triangle or a hexagon fragment) or if only one of the MoS_2 edges is active or available for promoter decoration. The calculated data can thus still be used to compare/rank the catalysts.

The promoter segregation was studied by STEM-EDX spectral imaging under analytical probe (1.0 nm) conditions, the result of which is a set of element maps. A (composite) element map gives qualitative information about the distribution of the element(s) by showing the total X-ray intensity within a specific energy range (Co-K, Ni-K, and Mo-K lines are chosen here) in each pixel. Metal sulfide particles must have a diameter of about 5 nm or more to be visible in the STEM-EDX maps under our measurement conditions. In spectral imaging, a complete EDX spectrum is acquired in each pixel of the map, which makes it possible to quantify the local composition by extraction of spectra from selected regions.

2.2.2. XRD

The samples were extracted with toluene prior to being powdered and measured with a PANalytical PW1050 reflection diffractometer with graphite monochromated Cu-K_α

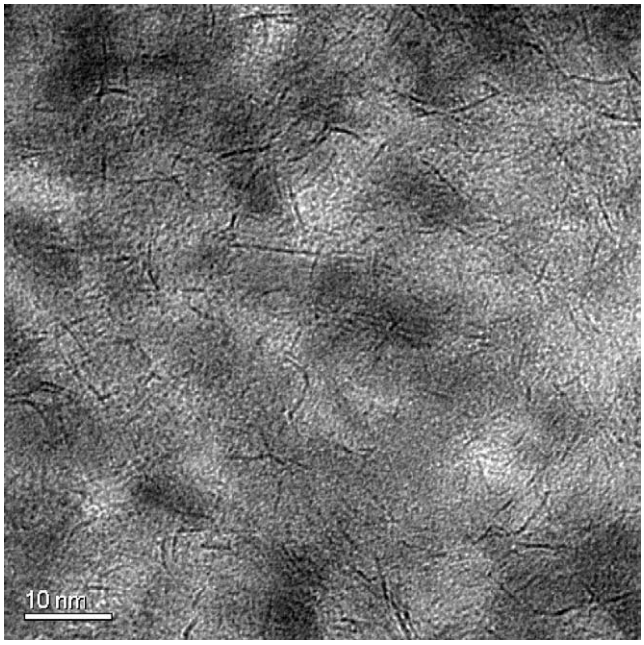

Fig. 1. TEM micrograph of liquid phase sulfided Type 2 Ni–Mo/Al_2O_3 catalyst NiMo3-T2-L-U.

radiation at 40 kV and 40 mA. A single silicon crystal was used as a sample holder. The XRD patterns were recorded with a step size of 0.02°. The Ni_3S_2 reflections were used as an internal standard for precise 2θ angle determination. The mean crystallite size (in Å) was determined with the Scherrer equation (with $k = 1$). Phase identification was checked with the use of the Powder Diffraction File from the International Centre for Diffraction Data (ICDD).

3. Results

3.1. Segregation of Ni sulfide

Commercial Types 1/2 and 2 Ni–Mo/Al_2O_3 hydroprocessing catalysts typically have a high MoS_2 dispersion, as measured by TEM [29,55]. Fig. 1 shows one example of the high MoS_2 dispersion of Type 2 Ni–Mo catalysts (NiMo3-T2-L-U). NiMo1-T2-L-F and NiMo2-T2-L-F catalysts have TEM characteristics similar to those of NiMo3-T2-L-U. The three catalysts contain predominantly short MoS_2 monolayers (Table 3).

Fig. 2 shows the XRD patterns of the NiMo1-T2-L-F and NiMo2-T2-L-F catalysts. Fig. 2 confirms the absence of significant MoS_2 stacking, since no clear MoS_2 peak is present at about $2\theta = 14°$. Aside from the features of low crystalline MoS_2 and γ-Al_2O_3, no crystalline phases were detected by XRD analysis of these samples. However, Ni_3S_2 crystals of various sizes could be observed by TEM. For example, in about 30% of the analyzed regions in NiMo1-T2-L-F (Fig. 3), Ni_3S_2 crystals are visible as dark and light spots in the bright-field and dark-field images, respectively. The identity of these crystals was verified by EDX analysis,

Table 3
MoS_2 dispersion calculated from TEM micrographs

Catalyst	Visualized [29,55]				Calculated [29,55]
	Stacks per 1000 nm^2	Average number of layers per stack	Average length (nm)	Visualized Mo (%)	Mo e + c[a] atoms per 10000 nm^3
NiMo1-T2-L-F	40	1.1	2.8	14	36300
NiMo2-T2-L-F	24	1.1	3.3	12	32000
NiMo3-T2-L-U	24	1.3	3.5	14	31600
NiMo3-T2-L-F/C	41	1.3	4.8	38	25500
NiMo3-T2-G-H	14	2.6	5.8	34	25500
CoMo1-T2-L-F	34	1.2	4.1	22	29800
CoMo2-T2-L-U	24	1.1	4.3	18	30600

[a] Edge + corner atoms (e + c). The accuracy of the calculated number of Mo e + c atoms is ±10% [55].

electron diffraction, and lattice imaging (Fig. 4a). Some of the Ni_3S_2 crystals are decorated with MoS_2 layers (Fig. 4b). A reference experiment was carried out to get an indication of the Ni_3S_2 detection limit in XRD. NiMo1-T2-L-F mixed with 1.5 wt% of crystalline bulk Ni_3S_2 (Aldrich; average crystallite size of about 70 nm obtained by the Scherrer equation, with the peak at about $2\theta = 22°$) was used as the reference sample. Small peaks of Ni_3S_2 were detected in this sample (Fig. 2).

STEM-EDX is an even more suitable element-specific technique for visualizing Ni sulfide particles (5–50 nm in diameter). Fig. 5 shows the results of the NiMo3-T2-L-U catalyst. NiMo1-T2-L-F and NiMo2-T2-L-F have similar STEM-EDX characteristics. From a comparison of the STEM-EDX data in areas without Ni-rich particles with the Ni bulk concentration it can be estimated that 32–47% of Ni has segregated in these catalysts. This corresponds to 1.3–3.0 wt% Ni_3S_2. When this information is combined with the MoS_2 dispersion calculated from the TEM micrographs (Table 3), using a method disclosed elsewhere [29,55], a still fairly high Ni edge occupation can be achieved. With about 80% of Mo atoms in edge and corner (e + c) positions, the remaining (not visibly segregated) Ni is still sufficient to reach Ni/Mo (e + c) atom ratios of 0.24–0.29. Ni sulfide segregation is also observed in Type 1/2 Ni–Mo catalysts. STEM-EDX analysis of a conventional mixed Type 1/2 Ni–Mo/Al_2O_3 catalyst, NiMo4-T1/2-L-F, shows that Ni-rich particles are clearly present (Fig. 6).

3.2. Differences between Ni–Mo and Co–Mo catalysts

No Co-rich particles are visible in Co–Mo Type 2 catalysts with the same composition and preparation, when they are used under the same conditions and have MoS_2 dispersions and morphologies (Table 3) to their Ni-containing counterparts. Fig. 7 shows the TEM and STEM-EDX results for CoMo2-T2-L-U. CoMo1-T2-L-F has comparable (S)TEM-EDX characteristics. CoMo2-T2-L-U (Fig. 7) can be directly compared with NiMo3-T2-L-U (Figs. 1 and 5). The same applies also to CoMo1-T2-L-F and NiMo2-T2-

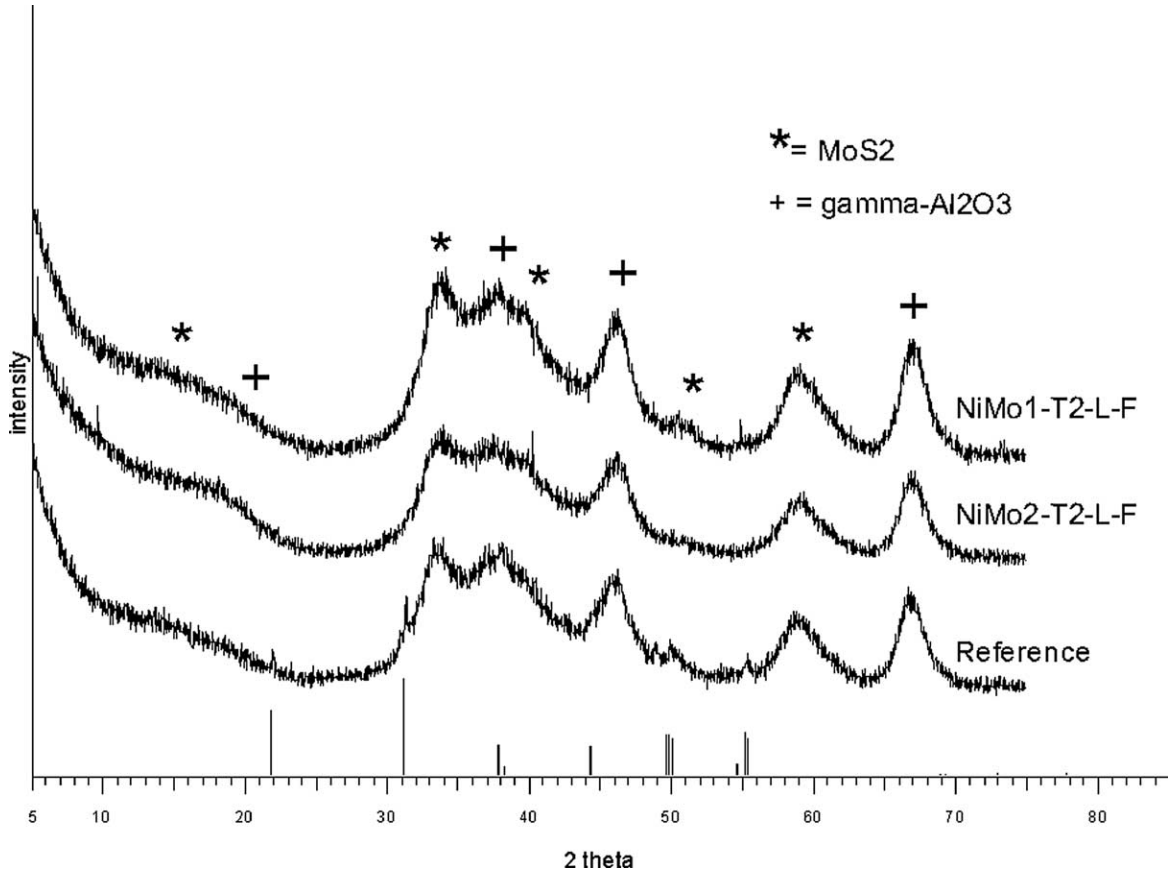

Fig. 2. XRD patterns of liquid phase sulfided Type 2 Ni–Mo/Al_2O_3 catalysts NiMo1-T2-L-F (top) and NiMo2-T2-L-F (middle) together with the pattern of a reference sample containing 1.5% Ni_3S_2 (bottom). The reference stick pattern of Ni_3S_2 is displayed at the bottom.

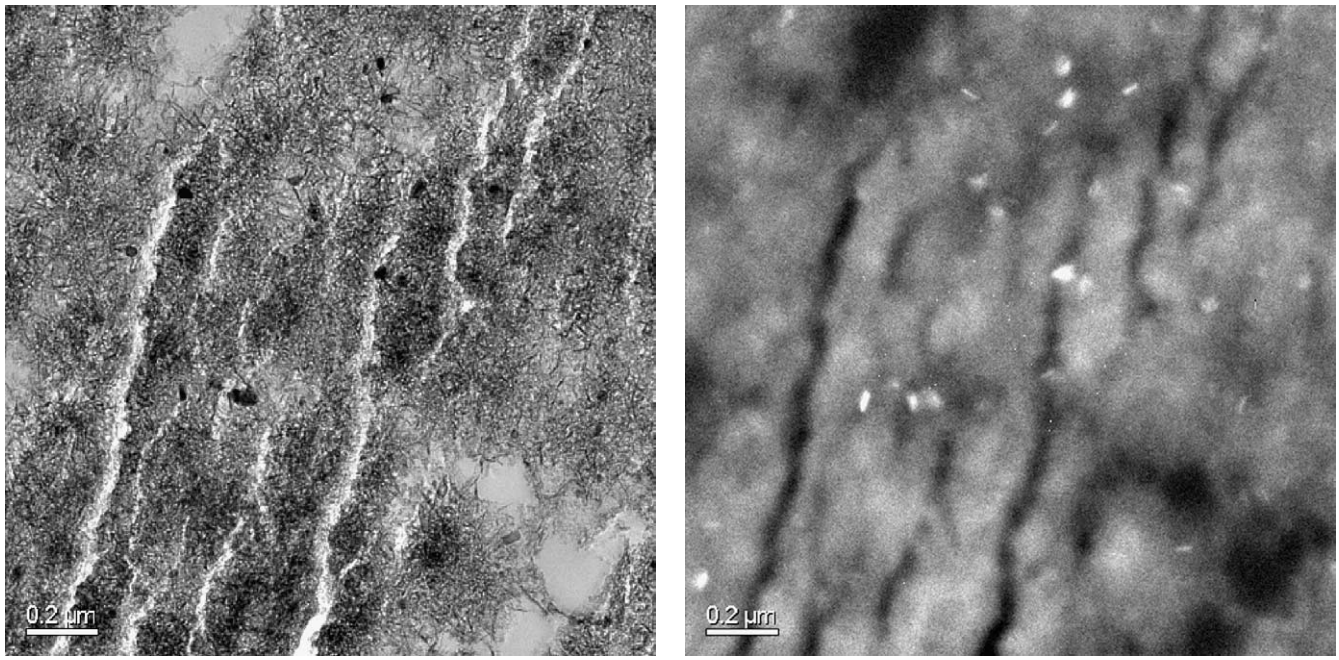

(a) (b)

Fig. 3. TEM micrographs of liquid phase sulfided Type 2 Ni–Mo/Al_2O_3 catalyst NiMo1-T2-L-F: (a) bright field and (b) corresponding dark field image (hollow cone illumination).

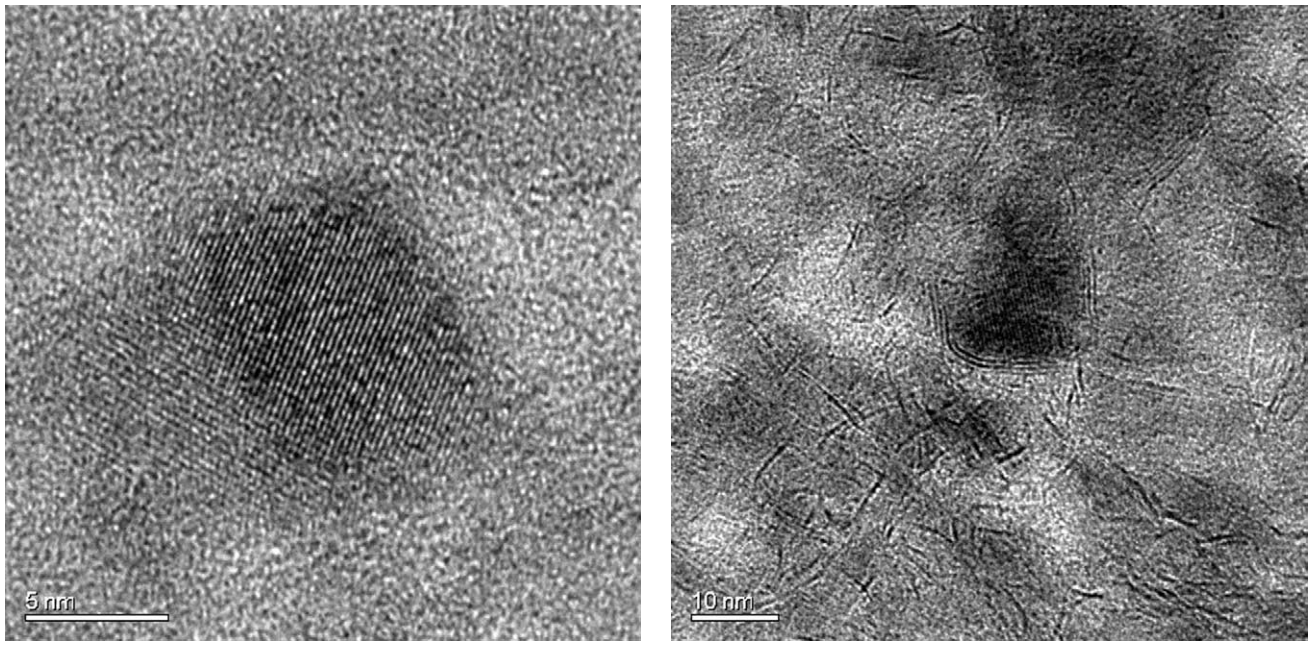

(a) (b)

Fig. 4. TEM micrographs of liquid phase sulfided Type 2 Ni–Mo/Al_2O_3 catalysts: (a) lattice image of a Ni sulfide particle in NiMo1-T2-L-F and (b) decoration of a Ni sulfide particle with MoS_2 slabs in NiMo2-T2-L-F.

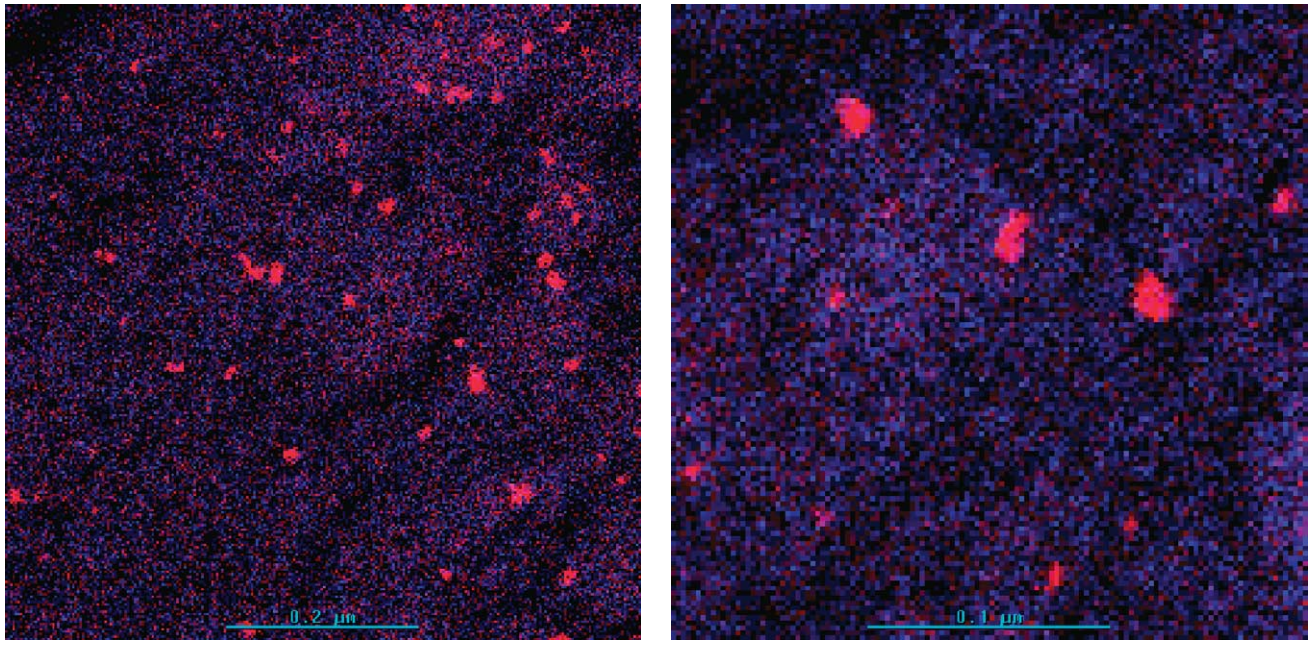

(a) (b)

Fig. 5. STEM-EDX composite images of Ni (red) and Mo (blue) maps of liquid phase sulfided Type 2 Ni–Mo/Al_2O_3 catalyst NiMo3-T2-L-U.

L-F catalysts, which are not shown in the figures. Co-rich particles are also not found in STEM-EDX maps of a conventional mixed Type 1/2 Co–Mo catalyst (CoMo3-T1/2-L-D). CoMo3-T1/2-L-D can be compared (similar composition and preparation) with NiMo4-T1/2-L-F (Fig. 6); however, the two catalysts originate from different tests.

3.3. Morphology of MoS_2

MoS_2 stacking does not dominate the images of liquid-phase-sulfided Type 2 commercial Ni–Mo catalysts and is almost completely absent in some cases (Fig. 1). The MoS_2 dispersion obtained depends on the sulfidation and reaction

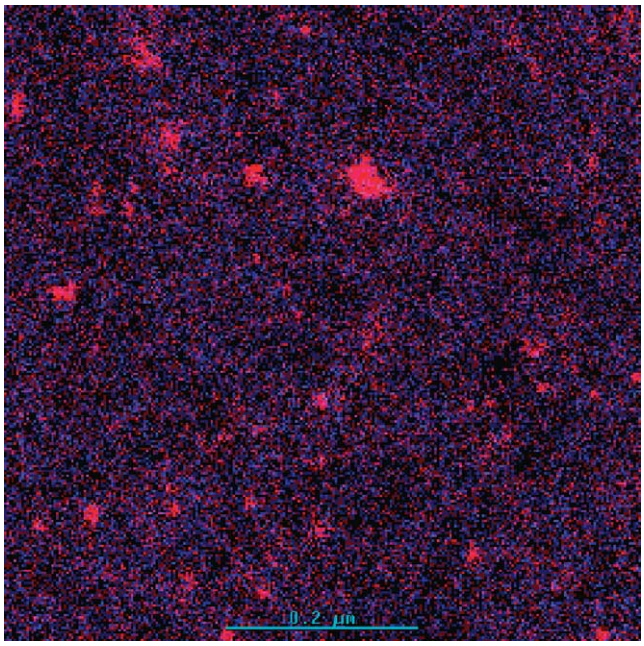

Fig. 6. STEM-EDX composite image of Ni (red) and Mo (blue) maps of liquid phase sulfided Type 1/2 Ni–Mo/Al_2O_3 catalyst NiMo4-T1/2-L-F.

conditions applied. Dispersion is typically high after liquid-phase sulfidation and with a short reaction time (Table 3, NiMo1-T2-L-F, NiMo2-T2-L-F, and NiMo3-T2-L-U). The MoS_2 slabs become longer (i.e., the dispersion is lower) if the same catalyst is used for a longer time and/or under more severe reaction conditions (Table 3, Fig. 8, NiMo3-T2-L-F/C). For example, NiMo3-T2-L-F/C was used for 1 year in a unit operating at high temperature. The degree of stacking is still rather limited, with most MoS_2 structures consisting of only one or two layers. In this particular case, another interesting feature becomes prominent, namely the curvature of the MoS_2 layers (Fig. 8). Other interesting MoS_2 morphologies regularly observed in Types 1 and 2 catalysts are Al_2O_3 needles/plates coated with MoS_2 (Fig. 9).

3.4. Effect of sulfidation procedure

Whereas MoS_2 stacking is not prominent where just liquid-phase sulfiding is carried out, curved MoS_2 stacks are formed after H_2S/H_2 sulfidation (Figs. 10a and b, Table 3, NiMo3-T2-G-H). The NiMo3-T2-G catalyst shows similar characteristics (Fig. 10c), also directly after 400 °C H_2S/H_2 sulfidation. The MoS_2 layers are only somewhat longer, but the average stack density is much lower after H_2S/H_2 sulfidation compared with liquid-phase sulfidation in combination with use under severe conditions (Table 3, Fig. 8, NiMo3-T2-L-F/C). That is why the two materials have the same MoS_2 dispersions (e + c atoms per 10000 nm^3). Even though smaller Ni-rich particles are not abundant in the gas-phase-sulfided catalyst NiMo3-T2-G-H, it contains some large Ni_3S_2 crystals (200 nm to 1 µm in diameter), which are also detected by XRD (Fig. 11). Another liquid-phase-sulfided NiMo3 sample with curved MoS_2 monolayers (with TEM characteristics similar to those of NiMo3-T2-L-F/C) exhibited only 5% higher hydrodenitrogenation (HDN) activity in the HC-PT test than NiMo3-T2-G-H with curved MoS_2 stacks. The performance ranking could be different, however, for HDS or hydrogenation and/or for other reaction conditions.

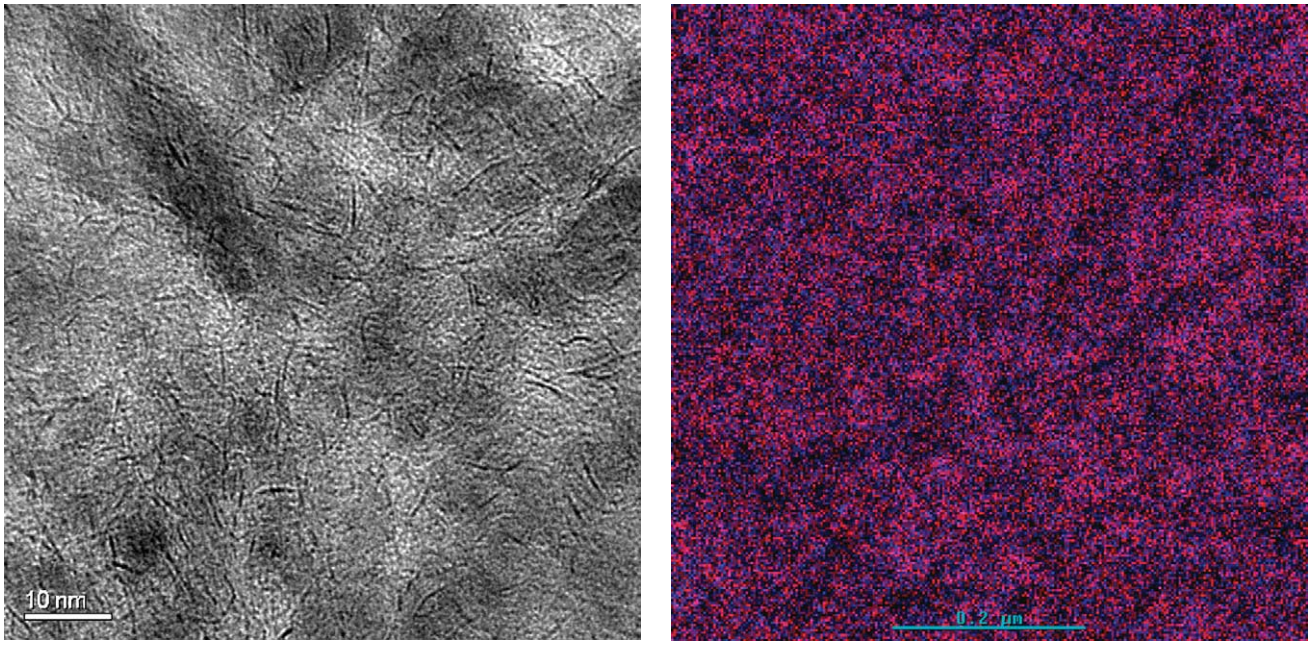

(a) (b)

Fig. 7. (a) TEM micrograph and (b) STEM-EDX composite image of Co (red) and Mo (blue) maps of liquid phase sulfided Type 2 Co–Mo/Al_2O_3 catalyst CoMo2-T2-L-U.

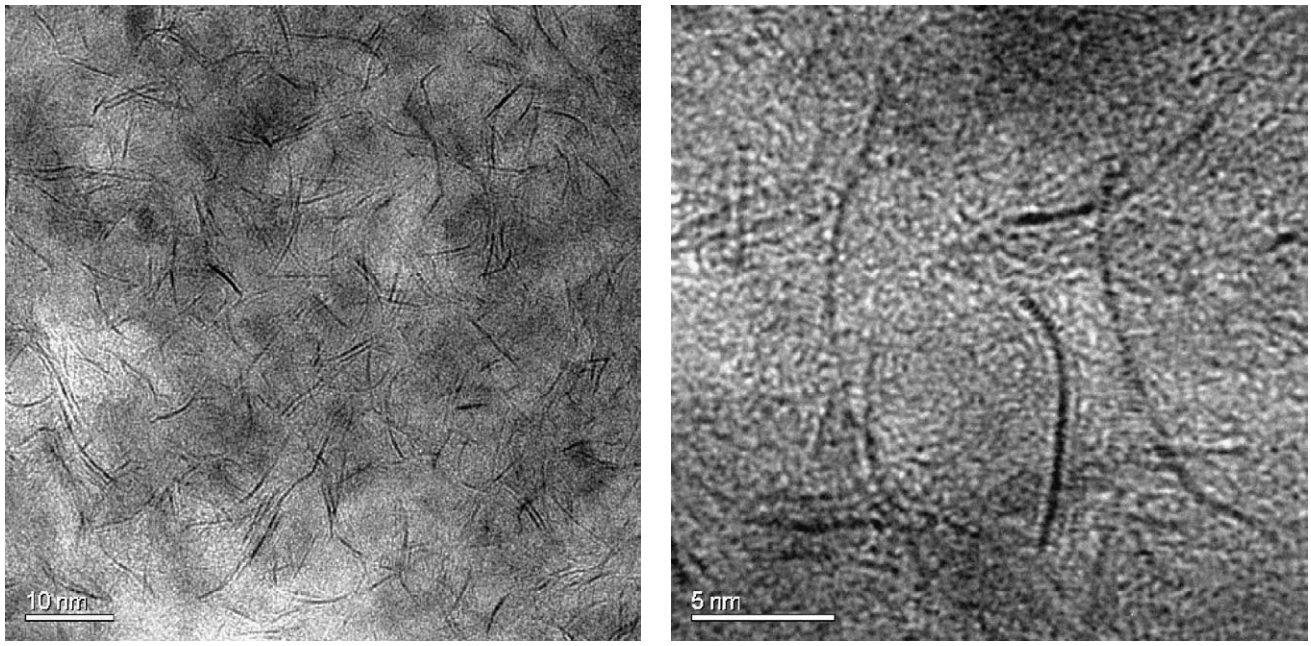

(a) (b)

Fig. 8. TEM micrographs of liquid phase sulfided Type 2 Ni–Mo/Al_2O_3 catalyst NiMo3-T2-L-F/C showing long curved MoS_2 slabs.

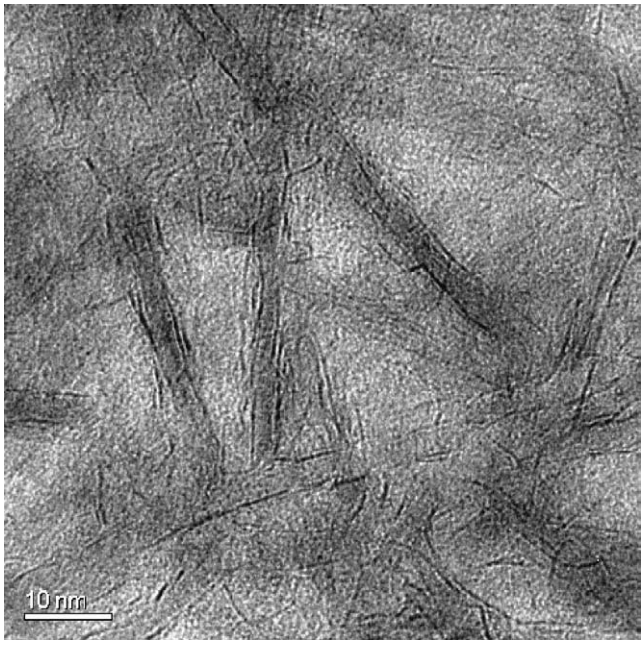

Fig. 9. TEM micrograph of liquid phase sulfided Type 2 Co–Mo/Al_2O_3 catalyst CoMo1-T2-L-F showing Al_2O_3 needles/plates coated with MoS_2.

XRD patterns of these samples contain contributions of Ni_3S_2 (only in NiMo3-T2-G-H), MoS_2, and γ-Al_2O_3 (Fig. 11). The absence of MoS_2 stacks in NiMo3-T2-L-F/C and the presence of MoS_2 stacks in NiMo3-T2-G-H are reflected in the absence/presence of the MoS_2 peak at about $2\theta = 14°$. This MoS_2 peak in NiMo3-T2-G-H is shifted to lower angles ($2\theta = 14.0°$) compared with the MoS_2 reference (ICDD 00-037-1492 MoS_2 molybdenite-2H; $2\theta = 14.4°$). This indicates *c*-axis expansion of the MoS_2 stacks in this catalyst.

4. Discussion

4.1. Segregation of Ni sulfide

Commercial Type 2 Ni–Mo/Al_2O_3 hydroprocessing catalysts that are liquid-phase sulfided typically have a high MoS_2 dispersion, as shown by TEM analysis (Fig. 1). Ni_3S_2 crystals (5–50 nm in diameter), some decorated with MoS_2 layers, are also present (Figs. 3 and 4). MoS_2 stacks and fewer but much larger (200 nm to 1 μm in diameter) Ni_3S_2 crystals are observed in TEM after gas-phase sulfidation. Ni sulfide segregation is also observed in Type 1/2 Ni–Mo catalysts. STEM-EDX spectral imaging is an element-specific technique for the study of element distributions and, therefore, a better tool for visualizing Ni sulfide particles [56,57] (Figs. 5 and 6). The amount of segregated Ni was estimated (from the STEM-EDX analysis) at about 32–47% of the total amount of Ni in the liquid-phase-sulfided Type 2 samples. The remaining (not visibly segregated) Ni is still sufficient to reach Ni/Mo e + c atom ratios of 0.24–0.29 (using the calculated MoS_2 dispersions [29,55]). This is low compared with the 0.5–1 values for high-dispersion (low-metal-loading) catalysts obtained with extended X-ray absorption fine structure (EXAFS) [4,10,11,58,59] or from performance studies where the promoter/molybdenum ratio was varied [60–65]. Nev-

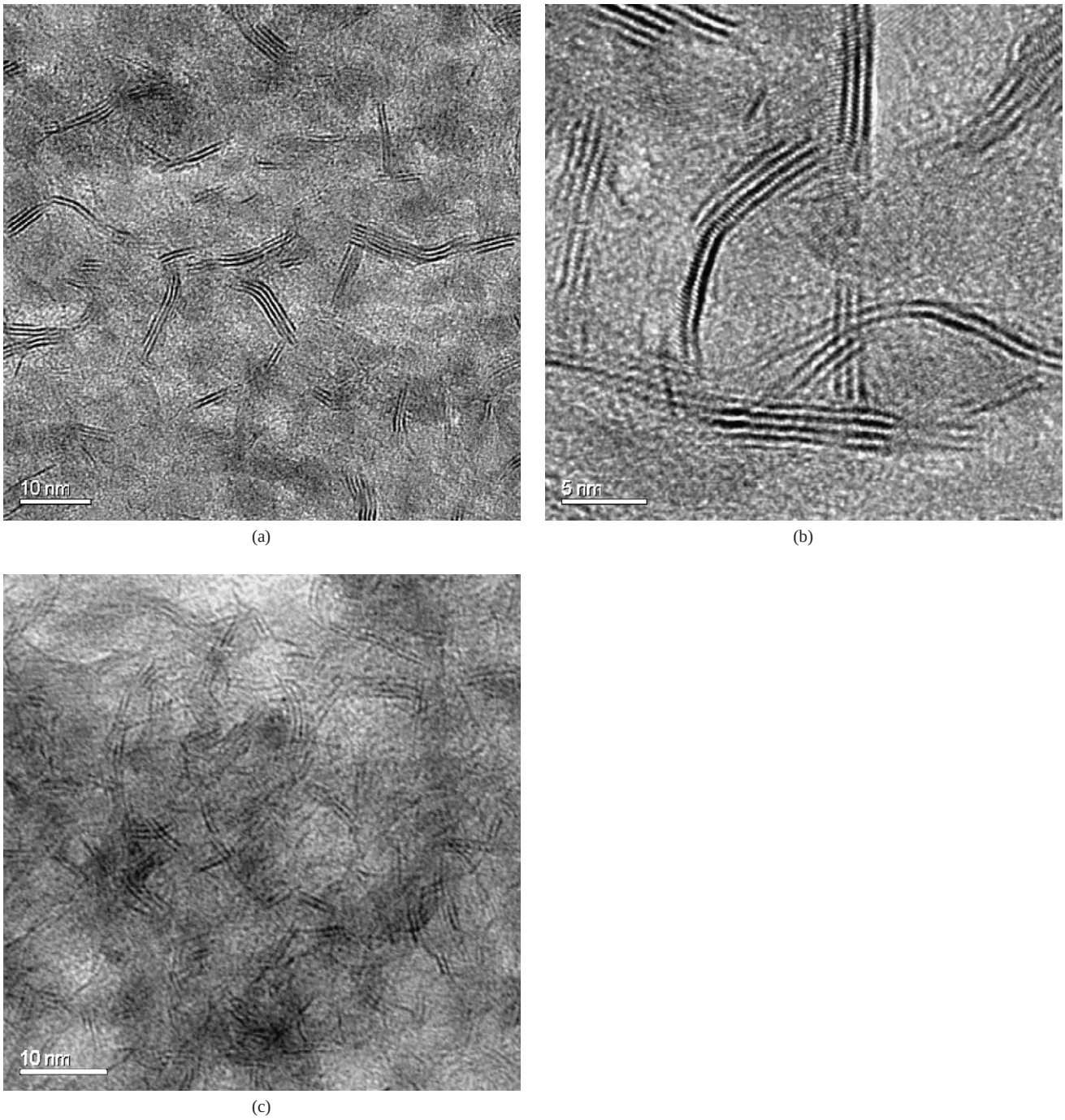

Fig. 10. TEM micrographs of gas phase sulfided Type 2 Ni–Mo/Al_2O_3 catalysts showing curved MoS_2 structures with significant stacking: (a) and (b) NiMo3-T2-G-H, and (c) NiMo3-T2-G.

ertheless, the 0.24–0.29 values are probably realistic for catalysts with this degree of Ni sulfide segregation and high metal surface loadings. Ni sulfide segregation is favored thermodynamically under the reaction conditions. It cannot be prevented but can only be slowed down by high initial dispersion and good Ni–Mo mixing. As proposed by the "Remote Control" model [26,30,38], the segregated Ni_3S_2 could make a positive contribution to catalytic performance.

4.2. *Detectability of Ni_3S_2 crystals in XRD*

Aside from the reflections of low-crystalline MoS_2 and γ-Al_2O_3, no crystalline phases were detected by XRD analysis of the liquid-phase-sulfided samples, despite the fact that they contained many small Ni sulfide particles, as shown by STEM-EDX analysis. In contrast to that, the few large segregated Ni_3S_2 crystals in the H_2S/H_2 sulfided catalyst are XRD detectable. A reference experiment shows that

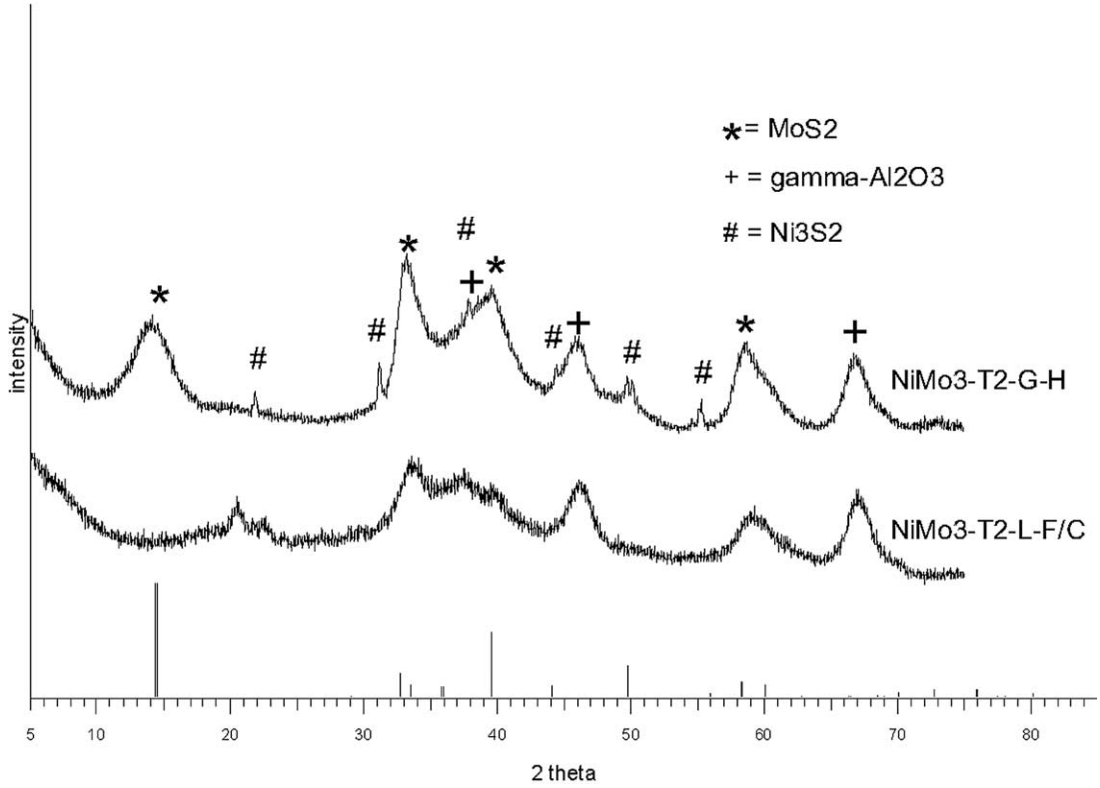

Fig. 11. XRD patterns of gas phase sulfided NiMo3-T2-G-H (top) and liquid phase sulfided NiMo3-T2-L-F/C (bottom) Type 2 Ni–Mo/Al_2O_3 catalysts. The reference stick pattern of MoS_2 is also displayed at the bottom.

1.5 wt% of crystalline bulk Ni_3S_2 (with an average crystallite size of about 70 nm) can be detected by XRD. The overall concentration of segregated Ni corresponds to about 1.3–3.0 wt% Ni_3S_2 in the liquid-phase-sulfided samples. Particle sizes between 5 and 50 nm are observed by TEM and STEM-EDX, although the average crystallite size (as probed by XRD) is probably at the lower level in this range. It has been shown for Ni steam-reforming catalysts that the Ni particle size observed by (S)TEM is larger than that obtained with XRD [66]. Apparently, the overall low concentration *in combination with* line broadening due to the small crystallite size makes the Ni_3S_2 crystals "invisible" in the XRD patterns of the liquid-phase-sulfided samples. Therefore, the absence of Ni_3S_2 peaks in the XRD pattern does not mean that there is no Ni sulfide segregation.

4.3. Differences between Ni–Mo and Co–Mo catalysts

No Co-rich particles are visible via STEM-EDX in commercial Type 2 Co–Mo/Al_2O_3 hydroprocessing catalysts with the same composition/preparation, when the catalysts are used under the same conditions and have a MoS_2 dispersion and morphology similar to those of their Ni-containing counterparts (Fig. 7). The commercial Type 1/2 Co–Mo/Al_2O_3 hydroprocessing catalysts do not contain Co-rich particles either. This suggests that a much higher promoter/Mo ratio may be required to cause promoter segregation in Co–Mo compared with Ni–Mo catalysts or that Co is more strongly bound to the MoS_2 edges than is Ni. However, these suggestions are not supported by data from the literature. Similar Ni/Mo and Co/Mo ratios are found to be optimum for catalyst performance in zeolite-supported [60,61], unsupported [62,63], and alumina-supported [64,65] materials. Moreover, EXAFS analysis indicates that Ni and Co sulfides decorating the MoS_2 edges have essentially the same coordination and distance to the nearest Mo atom [4,10,11,58,59]. Therefore, it is more probable that the absence of visible Co-rich particles is related to the fact that Co_9S_8 aggregates less rapidly than Ni_3S_2 because of its higher Tamman temperature (686 K for Co_9S_8 versus 532 K for Ni_3S_2) [56].

4.4. Morphology of MoS_2

MoS_2 stacking does not dominate the TEM images of liquid-phase-sulfided Type 2 commercial catalysts and is almost completely absent in some cases (Figs. 1 and 8, Table 3). This despite the fact that some of the catalysts are P-containing and MoS_2 stacking is often associated with the presence of P [67–69]. As the catalysts described in the present paper belong to the most active commercially available ULSD catalysts (and some of the samples actually originate from ULSD tests), it has to be concluded that MoS_2 stacking is not required for the desulfurization of molecules like 4,6-dialkyl dibenzothiophenes (DBT). This contradicts studies proposing that MoS_2 stacks are essential for 4,6-di-

alkyl DBT adsorption and/or catalysis of the hydrogenation pathway of 4,6-dialkyl DBT HDS [45,70].

Catalyst life-cycle studies have shown that MoS_2 dispersion is highly dependent on the sulfidation and reaction conditions applied [18,29,33,43,71,72]: MoS_2 slabs become longer (i.e., dispersion is lower) if the same catalyst is used for longer times and/or under more severe reaction conditions where the catalyst activity declines. In some cases, the long slabs are straight and apparently parallel to the support surface (Fig. 9). Long slabs oriented parallel to the support surface were also found in sulfided MgO-supported catalysts [73]. Curvature of the MoS_2 layers becomes prominent in certain samples used in high-severity applications, regardless of the presulfiding method used (Figs. 8 and 10). The fact that the curvature is visible is clearly related to the fact that the MoS_2 layers are very long in these samples [40,74].

Curved MoS_2 structures have often been observed in unsupported MoS_2-based catalysts [41,75], inorganic fullerenes (IF-Mo/WS_2) [76], and Mo sulfocarbides [42]. Several examples of MoS_2 layers "wrapped around" a support [45,77, 78] and Ni_3S_2 [79,80] and Co_9S_8 particles [48] have also been reported. So the curvature of the MoS_2 layers in the present samples can be attributed to the incorporation of C in the MoS_2 structure or to the fact that the layers are "wrapped around" Al_2O_3 and/or Ni_3S_2 particles. The tendency of MoS_2 to coat these substrates is also shown in the present set of data (Figs. 4b and 9). This is an indication that a significant part of the MoS_2 is, in fact, parallel to the support [39,46,47,49–53].

One should not misinterpret the term "parallel to" (i.e., following the contours of) the support as the presence of Mo–O–Al bonds or strong metal-support interaction when discussing Type 2 catalysts. The preparation of Type 2 catalysts prevents Mo–O–Al bonds from being formed, and, therefore, the MoS_2 phase is fully sulfided [19]. This means that weaker interactions such as van der Waals forces between the MoS_2 phase and the support surface [2] are responsible for the parallel orientation of the MoS_2 structures. The MoS_2 morphology and orientation are under further investigation with 3D-TEM measurements.

Expansion of the *c*-axis is observed in the XRD pattern of the catalyst containing curved MoS_2 stacks (Fig. 11, $2\theta = 14.0°$ instead of 14.4°, corresponding to an expansion of 0.3 Å). To our knowledge, this was reported only for unsupported MoS_2 [75,81–84]. The *c*-axis expansion was explained by strain effects, by the presence of defects involved in the folding of the MoS_2 layers [82], and by the formation of H_xMoS_2 by hydrogen intercalation in the van der Waals gaps [84]. It was proposed that in long curved MoS_2 structures the basal planes become accessible to reactant molecules [77,85] and that the defect sites are more active [41]. However, such a positive contribution of the curvature to the catalyst performance can probably only compensate for the simultaneous loss of MoS_2 dispersion due to long layers.

4.5. Effect of the sulfidation procedure

The present study clearly shows the impact of the sulfidation procedure on the Type 2 catalyst morphology. Whereas MoS_2 stacking is apparently enhanced by the H_2S/H_2 sulfidation (Fig. 10), liquid-phase sulfidation seems to prevent MoS_2 stacking (Figs. 1 and 8). Moreover, fewer but much larger Ni_3S_2 crystals are formed after H_2S/H_2 sulfidation than after liquid-phase sulfidation. Increased MoS_2 stacking due to H_2S/H_2 sulfidation was observed before [71]. This may be related to the exothermicity of H_2S/H_2 sulfidation [86–88], an effect that is suppressed if liquid is present and the heat of the sulfidation reaction is partly used to evaporate this liquid [89–91]. The prevention of stacking could also be related to the presence of hydrocarbons on the MoS_2 basal plane [92–96] in liquid-phase-sulfided samples.

The refinery practice highlights the goal of sulfidation, which is to bring the catalyst into equilibrium with its reaction environment in a controlled way [88,97] and not to achieve a complete sulfidation in the shortest possible period of time. The liquid-phase sulfidation procedure applied here is a mild sulfidation method (low heating rate, two steps, low final temperature, and presence of liquid) derived from a commercial refinery procedure. For practical reasons (time involved, high-pressure trickle-flow equipment availability), liquid-phase sulfidation has rarely been used in fundamental studies using model reactions, in short screening tests, or when contamination of analytical equipment with hydrocarbons must be prevented. The typical H_2S/H_2 sulfidation [86–88] is usually a very severe method (high heating rate, one step, high final temperature of 400 °C, and absence of liquid) that is primarily used because of its convenience (fast, simple atmospheric pressure gas-phase equipment). Mild sulfidation, however, is not a guarantee that MoS_2 stacks will be absent in all cases. There are several examples of liquid-phase-sulfided Type 1/2 catalysts that contain MoS_2 stacks [29,71]. This is probably related to the cluster size of the Mo precursor prior to sulfidation, which is apparently larger in the calcined Type 1/2 than in the Type 2 precursors.

The results of the liquid-phase-sulfided Type 2 catalysts demonstrate that lower active phase-support interaction, induced either by Type 2 preparation and/or by the presence of phosphorus, does not necessarily lead to MoS_2 stacking, provided the catalysts are sulfided under mild conditions. All samples studied in the present paper contain P (0.3 to 4.5 at/nm^2). Yet, with the exception of the H_2S sulfided sample, MoS_2 stacking is essentially absent: that is, there is no distinct relationship between the P content and MoS_2 stacking in this series of catalysts. This indicates that the lower metal-support interaction introduced by P leads to MoS_2 stacking only if other conditions are met as well (e.g., complete sulfidation and high reaction exotherm). The results for the canister sample further show that the degree of stacking remains low even if the liquid-phase-sulfided catalyst is used for a long period of time and under high-severity conditions.

It may therefore be argued that the direct link of Type 2 active phase with MoS_2 stacking [1,3–7,17,18] is, in fact, circumstantial. It is a consequence of the higher mobility of the active phase in Type 2 catalysts (due to the absence of Mo–O–Al linkages) *in combination with* the severe H_2S/H_2 sulfidation. This phenomenon may be quite unimportant in commercial refinery units, which mostly apply liquid-phase sulfidation. Samples with (curved) MoS_2 monolayers and those with (curved) MoS_2 stacks can have similar overall MoS_2 dispersions and, consequently, similar activities. So the MoS_2 stacking is neither a prerequisite for a good performance nor a sign of deactivation or lower activity.

5. Conclusions

I. Commercial Type 2 Ni–Mo/Al_2O_3 liquid-phase-sulfided hydroprocessing catalysts typically exhibit a high MoS_2 dispersion. However, a significant part of Ni segregates and is present as separate Ni-rich particles. The remaining (not visibly segregated) Ni is still sufficient for moderately high Ni/Mo edge + corner atom ratios. The Ni sulfide segregation is also observed in Type 1/2 Ni–Mo catalysts. Most importantly, the absence of Ni_3S_2 peaks in the XRD pattern does not indicate the absence of Ni sulfide segregation.

II. No Co-rich particles are visible in commercial Type 2 Co–Mo/Al_2O_3 hydroprocessing catalysts with the same composition/preparation, when they are used under the same conditions and have a MoS_2 dispersion and morphology similar to those of their Ni-containing counterparts. Also commercial Type 1/2 Co–Mo/Al_2O_3 hydroprocessing catalysts contain no Co-rich particles. This is probably due to the fact that Co_9S_8 aggregates less rapidly than Ni_3S_2.

III. MoS_2 stacking does not dominate the TEM images of liquid-phase-sulfided Type 2 commercial ULSD catalysts and is almost completely absent in some cases. MoS_2 stacking is thus not required for the desulfurization of molecules like 4,6-dialkyl DBT.

IV. The MoS_2 slabs become longer and are sometimes curved in catalysts used for a longer time and/or under more severe reaction conditions. The curvature may be an indication that a significant part of MoS_2 is parallel to the support but does not necessarily make any positive contribution to the catalyst's performance.

V. The sulfidation procedure has a significant impact on the Type 2 catalyst morphology. Whereas MoS_2 stacking is apparently enhanced by H_2S/H_2 sulfidation, liquid-phase-sulfidation seems to prevent it. Fewer but much larger Ni_3S_2 crystals are formed after H_2S/H_2 sulfidation than after liquid-phase sulfidation. This may be related to the exothermicity of the H_2S/H_2 sulfidation, an effect that is suppressed if liquid is present during the sulfidation.

VI. The goal of the sulfidation is to bring the catalyst in equilibrium with its reaction environment in a controlled way and not to achieve a complete sulfidation in the shortest possible period of time. In contrast to the mild liquid-phase sulfidation procedure, typical H_2S/H_2 sulfidation is very severe.

VII. Lower active phase-support interaction, induced either by Type 2 preparation and/or by the presence of phosphorus, does not necessarily lead to MoS_2 stacking, provided the catalysts are sulfided under mild conditions.

VIII. The direct link of the Type 2 active phase with MoS_2 stacking proposed in the literature may be circumstantial. It is a consequence of the higher mobility of the active phase in Type 2 catalysts *in combination with* severe H_2S/H_2 sulfidation. This phenomenon may be unimportant in commercial units using liquid-phase sulfidation. MoS_2 stacking is neither a prerequisite for a good performance nor a sign of deactivation or lower activity.

Acknowledgment

The authors thank Mrs. Caroline van der Meij for the TEM sample preparation.

References

[1] H. Topsøe, B.S. Clausen, Catal. Rev.-Sci. Eng. 26 (1984) 395.
[2] J.A.R. van Veen, E. Gerkema, A.M. van der Kraan, A. Knoester, J. Chem. Soc. Chem. Commun. 22 (1987) 1684.
[3] J.A.R. van Veen, H.A. Colijn, P.A.J.M. Hendriks, A.J. van Welsenes, Fuel Proc. Technol. 35 (1993) 137.
[4] S.M.A.M. Bouwens, M.P. van Dijk, A.M. van der Kraan, D.C. Koningsberger, F.B.M. van Zon, V.H.J. de Beer, J.A.R. van Veen, J. Catal. 146 (1994) 375.
[5] R. Candia, B.S. Clausen, H. Topsøe, in: M.F. Portela, et al. (Eds.), Proc. 9th Ibero-American Symp. on Catalysis Lisbon, Portugal, 1984, p. 211.
[6] R. Candia, O. Sørensen, J. Villadsen, N.-Y. Topsøe, B.S. Clausen, H. Topsøe, Bull. Soc. Chim. Belg. 93 (1984) 763.
[7] H. Topsøe, R. Candia, N.-Y. Topsøe, B.S. Clausen, Bull. Soc. Chim. Belg. 93 (1984) 783.
[8] E.J.M. Hensen, V.H.J. de Beer, J.A.R. van Veen, R.A. van Santen, Catal. Lett. 84 (2002) 59.
[9] J.A.R. van Veen, E. Gerkema, A.M. van der Kraan, P.A.J.M. Hendriks, H.J. Beens, J. Catal. 133 (1992) 112.
[10] S.M.A.M. Bouwens, J.A.R. van Veen, D.C. Koningsberger, V.H.J. de Beer, R. Prins, J. Phys. Chem. 95 (1991) 123.
[11] S.P.A. Louwers, R. Prins, J. Catal. 133 (1992) 94.
[12] R. Cattaneo, F. Rota, R. Prins, J. Catal. 199 (2001) 318.
[13] R. Cattaneo, T. Weber, T. Shido, R. Prins, J. Catal. 191 (2000) 225.
[14] Y. Okamoto, S. Ishihara, M. Kawano, M. Satoh, T. Kubota, J. Catal. 217 (2003) 12.
[15] A.J. van Dillen, R.J.A.M. Terörde, D.J. Lensveld, J.W. Geus, K.P. de Jong, J. Catal. 216 (2003) 257.
[16] L. Coulier, V.H.J. de Beer, J.A.R. van Veen, J.W. Niemantsverdriet, J. Catal. 197 (2001) 26.
[17] H. Topsøe, B.S. Clausen, N.Y. Topsøe, P. Zeuthen, Stud. Surf. Sci. Catal. 53 (1990) 77.

[18] S. Eijsbouts, Appl. Catal. A 158 (1997) 53.
[19] S. Eijsbouts, F.L. Plantenga, R.G. Leliveld, Y. Inoue, K. Fujita, Prepr. ACS Div. Fuel Chem. 48 (2003) 494.
[20] L.A. Gerritsen, S. Eijsbouts, Y. Inoue, P.H. Desai, Hydrocarbon Eng. 4 (1999) 46.
[21] Y. Inoue, Y. Uragami, S. Eijsbouts, Y. Takahashi, Stud. Surf. Sci. Catal. 121 (1999) 415.
[22] R.R. Chianelli, M. Daage, Prepr. ACS Div. Petrol. Chem. 35 (1990) 69.
[23] R. Prins, Charact. Catal. Mater. (1992) 109.
[24] J. Grimblot, Catal. Today 41 (1998) 111.
[25] M. Breysse, P. Afanasiev, C. Geantet, M. Vrinat, Catal. Today 86 (2003) 5.
[26] M. Karroua, H. Matralis, E. Sham, P. Grange, B. Delmon, Bull. Chem. Soc. Jap. 68 (1995) 107.
[27] T.I. Koranyi, G. De Vries, X. Lun, Z. Paal, Catal. Today 5 (1989) 185.
[28] J.R. Guenter, T.I. Koranyi, O. Marks, Z. Paal, Appl. Catal. 39 (1988) 285.
[29] S. Eijsbouts, J.J.L. Heinerman, H.J.W. Elzerman, Appl. Catal. A 105 (1993) 69.
[30] M. Karroua, H. Matralis, P. Grange, B. Delmon, Bull. Soc. Chim. Belg. 104 (1995) 11.
[31] S. Eijsbouts, J.N.M. van Gestel, J.A.R. van Veen, V.H.J. de Beer, R. Prins, J. Catal. 131 (1991) 412.
[32] L. Zhang, G. Karakas, U.S. Ozkan, J. Catal. 178 (1998) 457.
[33] S. Eijsbouts, Y. Inoue, Stud. Surf. Sci. Catal. 92 (1995) 429.
[34] S.M.A.M. Bouwens, N. Barthe-Zahir, V.H.J. de Beer, R. Prins, J. Catal. 131 (1991) 326.
[35] L.I. Pavlova, D.A. Agievskii, M.V. Landau, V.I. Kvashonkin, G.D. Chukin, B.K. Nefedov, Kinet. Katal. 29 (1988) 1457.
[36] D.A. Agievskii, L.I. Pavlova, V.I. Kvashonkin, Kinet. Katal. 31 (1990) 1268.
[37] J.V. Sanders, K.C. Pratt, J. Catal. 67 (1981) 331.
[38] M. Karroua, H. Matralis, P. Grange, B. Delmon, J. Catal. 139 (1993) 371.
[39] R.M. Stockman, H.W. Zandbergen, A.D. van Langeveld, J.A. Moulijn, J. Mol. Catal. A 102 (1995) 147.
[40] L.-S. Kao, D.R. Peacor, R.M. Coveney, Jr. Zhao, D. Gengmei, E. Keenan, M.D. Curtis, J.E. Penner-Hahn, Am. Mineralogist 86 (2001) 852.
[41] Y. Iwata, Y. Miki, K. Sato, T. Yoneda, Y. Sugimoto, A. Nishijima, H. Shimada, Catal. Today 45 (1998) 353.
[42] G. Berhault, L.C. Araiza, A.D. Moller, A. Mehta, R.R. Chianelli, Catal. Lett. 78 (2002) 81.
[43] N. Yueqin, Z. Yan, Z. Jingling, W. Jifeng, Stud. Surf. Sci. Catal. 88 (1994) 401.
[44] Y. Sakashita, Y. Araki, K. Honna, H. Shimada, Appl. Catal. A 197 (2000) 247.
[45] E.J.M. Hensen, P.J. Kooyman, Y. van der Meer, A.M. van der Kraan, V.H.J. de Beer, J.A.R. van Veen, R.A. van Santen, J. Catal. 199 (2001) 224.
[46] K.C. Pratt, J.V. Sanders, V. Christov, J. Catal. 124 (1990) 416.
[47] S. Srinivasan, A.K. Datye, C.H.F. Peden, J. Catal. 137 (1992) 513.
[48] K. Inamura, R. Prins, J. Catal. 147 (1994) 515.
[49] Y. Sakashita, T. Yoneda, J. Catal. 185 (1999) 487.
[50] Y. Sakashita, Y. Araki, H. Shimada, Appl. Catal. A 215 (2001) 101.
[51] Y. Araki, K. Honna, H. Shimada, J. Catal. 207 (2002) 361.
[52] T.F. Hayden, J.A. Dumesic, J. Catal. 103 (1987) 366.
[53] F. Delannay, Appl. Catal. 16 (1985) 135.
[54] A. Ionescu, A. Allouche, J.-P. Aycard, M. Rajzmann, R. Le Gall, J. Phys. Chem. B 107 (2003) 8490.
[55] S. Eijsbouts, J.J.L. Heinerman, H.J.W. Elzerman, Appl. Catal. A 105 (1993) 53.
[56] X. Zhao, J. Wei, J. Catal. 147 (1994) 429.
[57] E. Freund, J. Lynch, R. Szymanski, Ultramicroscopy 20 (1986) 107.
[58] W. Niemann, B.S. Clausen, H. Topsøe, Catal. Lett. 4 (1990) 355.
[59] M.W.J. Craje, V.H.J. de Beer, J.A.R. van Veen, A.M. van der Kraan, Chem. Ind. (Dekker) 67 (1996) 95.
[60] A. Wang, Y. Wang, T. Kabe, Y. Chen, A. Ishihara, W. Qian, P. Yao, J. Catal. 210 (2002) 319.
[61] Y. Okamoto, H. Katsuyama, AIChE J. 43 (1997) 2809.
[62] M.O. Alias, V. Srinivasan, Hung. J. Ind. Chem. 20 (1992) 161.
[63] T.I. Koranyi, O. Marks, I. Manninger, Z. Paal, J.R. Guenter, J. Catal. 116 (1989) 422.
[64] W. Quian, A. Ishihara, Y. Okoshi, W. Nakakami, M. Godo, T. Kabe, J. Chem. Soc. Faraday Trans. 93 (1997) 4395.
[65] W. Quian, A. Ishihara, Y. Aoyama, T. Kabe, Appl. Catal. A 196 (2000) 103.
[66] J. Sehested, A. Carlsson, T.V.W. Janssens, P.L. Hansen, A.K. Datye, J. Catal. 197 (2001) 200.
[67] R.C. Ryan, R.A. Kemp, J.A. Smegal, D.R. Denley, G.E. Spinnler, Stud. Surf. Sci. Catal. 50 (1989) 21.
[68] R.A. Kemp, R.C. Ryan, J.A. Smegal, in: M.J. Philips, M. Ternan (Eds.), Proceedings 9th Int. Congress on Catalysis, Calgary, vol. 1, The Chemical Institute of Canada, Ottawa, 1988, p. 128.
[69] R. Iwamoto, J. Grimblot, Adv. Catal. 44 (1999) 417.
[70] H. Qabazard, F. Abu-Seedo, A. Stanislaus, M. Andari, M. Absi-Halabi, Fuel Sci. Technol. Int. 13 (1995) 1135.
[71] Y. Tanaka, H. Shimada, M. Matsubayashi, A. Nishijima, M. Nomura, Catal. Today 45 (1998) 319.
[72] Y. Yokoyama, N. Ishikawa, K. Nakanishi, K. Satoh, Catal. Today 29 (1996) 261.
[73] J. Cinibulk, P.J. Kooyman, Z. Vit, M. Zdražil, Catal. Lett. 89 (2003) 147.
[74] R.R. Chianelli, A.F. Ruppert, M.J. Yacaman, A. Vazquez-Zavala, Catal. Today 23 (1995) 269.
[75] M.M. Mdleleni, T. Hyeon, K.S. Suslick, J. Am. Chem. Soc. 120 (1998) 6189.
[76] R. Tenne, L. Margulis, M. Genut, G. Hodes, Nature 360 (1992) 444.
[77] A.K. Datye, S. Srinivasan, L.F. Allard, C.H.F. Peden, J.R. Brenner, L.T. Thompson, J. Catal. 158 (1996) 205.
[78] J.V. Sanders, J. Electron Mic. Techn. 3 (1986) 67.
[79] F. Pedraza, S. Fuentes, Catal. Lett. 65 (2000) 107.
[80] F.B. Garreau, H. Toulhoat, S. Kasztelan, R. Paulus, Polyhedron 5 (1986) 211.
[81] K.S. Liang, R.R. Chianelli, F.Z. Chien, S.C. Moss, J. Non-Cryst. Solids 79 (1986) 251.
[82] Y. Feldman, E. Wasserman, D.J. Srolovitz, R. Tenne, Science 267 (1995) 222.
[83] M. Chhowalla, G.A.J. Amaratunga, Nature 407 (2000) 164.
[84] C.J. Wright, C. Sampson, D. Fraser, R.B. Moyes, P.B. Wells, C. Riekel, J.C.S. Faraday I 76 (1980) 1585.
[85] D.I. Kochubey, V.P. Babenko, React. Kinet. Catal. Lett. 77 (2002) 237.
[86] S. Blashka, G. Bond, D. Ward, Oil Gas J. 96 (1998) 36.
[87] P. Raybaud, H. Toulhoat, J. Hafner, G. Kresse, S. Kasztelan, J. Catal. 189 (2000) 129.
[88] T.C. Ho, S.C. Reyes, Chem. Eng. Sci. 45 (1990) 2633.
[89] P. Dufresne, F. Labruyere, EP993868 (2000).
[90] P. Dufresne, S. Eijsbouts, F. Labruyere, F.L. Plantenga WO200176741 (2000).
[91] H. Hallie, Oil Gas J. 80 (1982) 69.
[92] C. Glasson, C. Geantet, M. Lacroix, F. Labruyère, P. Dufresne, J. Catal. 212 (2002) 6.
[93] J. van Doorn, J.A. Moulijn, G. Djega-Mariadassou, Appl. Catal. 63 (1990) 77.
[94] Y. Peng, Z. Meng, C. Zhong, J. Lu, W. Yu, Z. Yang, Y. Qian, J. Solid State Chem. 159 (2001) 170.
[95] M.P. de la Rosa, S. Texier, G. Berhault, A. Camacho, M.J. Yacaman, A. Mehta, S. Fuentes, J.A. Montoya, F. Murrietta, R.R. Chianelli, J. Catal. 225 (2004) 288.
[96] G. Berhault, A. Mehta, P. Apurva, C. Alexandru, J. Yang, L. Rendon, M.J. Yacaman, L.C. Araiza, A.D. Moller, R.R. Chianelli, J. Catal. 198 (2001) 9.
[97] R. Marinkovic-Neducin, J. Kiurski, K. Djurdjevic, R. Micic, Pet. Coal 41 (1999) 163.